Functional Divergence in Solute Permeability between Ray-Finned Fish-Specific Paralogs of *aqp10*

Genki Imaizumi[1,†], Kazutaka Ushio [1,†], Hidenori Nishihara [1,2], Ingo Braasch [3], Erika Watanabe[1], Shiori Kumagai[1], Tadaomi Furuta [1], Koji Matsuzaki [4], Michael F. Romero [5,6], Akira Kato [1,*], and Ayumi Nagashima [1,*]

[1]School of Life Science and Technology, Tokyo Institute of Technology, Yokohama, Japan

[2]Department of Advanced Bioscience, Faculty of Agriculture, Kindai University, Nara, Japan

[3]Department of Integrative Biology and Ecology, Evolution, and Behavior Program, College of Natural Science, Michigan State University, East Lansing, Michigan, USA

[4]Marine Science Museum, Fukushima Prefecture (Aquamarine Fukushima, AMF), Iwaki, Japan

[5]Department of Physiology and Biomedical Engineering, Mayo Clinic College of Medicine & Science, Rochester, Minnesota, USA

[6]Department of Nephrology and Hypertension, Mayo Clinic College of Medicine & Science, Rochester, Minnesota, USA

*Corresponding authors: E-mails: akirkato@bio.titech.ac.jp; anagashima@bio.titech.ac.jp.

[†]These authors contributed equally as the first authors.

Accepted: November 22, 2023

Abstract

Aquaporin (Aqp) 10 is a member of the aquaglyceroporin subfamily of water channels, and human Aqp10 is permeable to solutes such as glycerol, urea, and boric acid. Tetrapods have a single *aqp10* gene, whereas ray-finned fishes have paralogs of this gene through tandem duplication, whole-genome duplication, and subsequent deletion. A previous study on Aqps in the Japanese pufferfish *Takifugu rubripes* showed that one pufferfish paralog, Aqp10.2b, was permeable to water and glycerol, but not to urea and boric acid. To understand the functional differences of Aqp10s between humans and pufferfish from an evolutionary perspective, we analyzed Aqp10s from an amphibian (*Xenopus laevis*) and a lobe-finned fish (*Protopterus annectens*) and Aqp10.1 and Aqp10.2 from several ray-finned fishes (*Polypterus senegalus*, *Lepisosteus oculatus*, *Danio rerio*, and *Clupea pallasii*). The expression of tetrapod and lobe-finned fish Aqp10s and Aqp10.1-derived Aqps in ray-finned fishes in *Xenopus* oocytes increased the membrane permeabilities to water, glycerol, urea, and boric acid. In contrast, Aqp10.2-derived Aqps in ray-finned fishes increased water and glycerol permeabilities, whereas those of urea and boric acid were much weaker than those of Aqp10.1-derived Aqps. These results indicate that water, glycerol, urea, and boric acid permeabilities are plesiomorphic activities of Aqp10s and that the ray-finned fish-specific Aqp10.2 paralogs have secondarily reduced or lost urea and boric acid permeability.

Key words: aquaporin 10, aquaglyceroporin, paralog, ray-finned fish, subfunctionalization, neofunctionalization.

Introduction

Aquaporins (Aqps) are a family of water channel proteins that contain six-transmembrane domains (Borgnia et al. 1999; Agre et al. 2002; Azad et al. 2021) (Note that, in this article, protein names of all species are shown with the first letter capitalized rather than the full name italicized and gene names of all species are shown as lowercase and italicized). Most mammals, including human, possess 13 members of the aquaporin family (Aqp0–12), of which Aqp3, 7, 9, and 10 transport small, uncharged solutes, such as glycerol and urea, in addition to water. These four proteins are grouped into the aquaglyceroporin subfamily. The *aqp10* gene of certain rodents (e.g., mice) and ruminants (e.g., cows, sheep, and goats) has been

Significance

Aquaporin (Aqp) 10 is a member of the aquaglyceroporin subfamily transporting small, uncharged solutes in addition to water. Differences in the solute permeabilities of Aqp10s between tetrapods and fishes have been identified, but it remains unclear when and how these differences arose. Water, glycerol, urea, and boric acid permeability was suggested as a plesiomorphic activity of Aqp10s and was conserved in Aqp10s of a tetrapod, a lobe-finned fish, and the Aqp10.1 paralogs in ray-finned fishes. On the other hand, the permeabilities of the Aqp10.2 paralogs to urea and boric acid were much weaker than those of plesiomorphic Aqp10s. This difference in activity between the specific Aqp10 paralogs of ray-finned fish suggests functional divergence following their tandem gene duplication.

lost or transitioned to a pseudogene (Morinaga et al. 2002; Tanaka et al. 2015). Studies on the Aqp8s of humans and fishes indicate that this protein is also permeable to water and small uncharged molecules such as urea, but not to glycerol; therefore, Aqp8 is categorized as a member of the water and urea channel subfamily (Tingaud-Sequeira et al. 2010; Ushio et al. 2022; Kumagai et al. 2023). In contrast, Aqp1, 2, 4, and 5 are permeable to water but not to glycerol, urea, or other compounds, and these Aqps are categorized as classical or water-selective.

Aquaglyceroporins in mammals are involved in physiological processes such as gastrointestinal functioning, hepatic and adipocyte metabolism, skin elasticity, and pancreatic β-cell regulation (Lebeck 2014; Laforenza et al. 2016; Calamita and Delporte 2021). Their expression differs by location: Aqp7 and 10 in the apical membrane of enterocytes, Aqp3 in the basolateral membrane of enterocytes, Aqp9 in the plasma membrane of hepatocytes, and Aqp3, 7, 9, and 10 in adipose tissue. These aquaglyceroporins play significant roles in glycerol metabolism. In addition, Aqp3 is expressed in various tissues, including epidermal keratinocytes. In Aqp3-deficient mice, the epidermis has reduced water and glycerol content in the stratum corneum, reduced skin elasticity, impaired epidermal biosynthesis, and delayed wound healing (Hara-Chikuma and Verkman 2008). Aqp7 is also expressed in pancreatic β-cells, and Aqp7-mediated glycerol uptake is involved in β-cell insulin secretion (Matsumura et al. 2007).

Detailed analyses of the Aqp superfamily in vertebrates (Finn et al. 2014; Finn and Cerda 2015; Chauvigne et al. 2019; Yilmaz et al. 2020) revealed 17 subfamilies (Aqp0–16), of which Aqp3, 7, 9, 10, and 13 belong to the subfamily aquaglyceroporins. Aqp3, 7, 9, and 10 are present in a relatively large number of species, whereas Aqp13 is present only in prototherian mammals and in amphibians (Finn et al. 2014; Finn and Cerda 2015; Chauvigne et al. 2019; Yilmaz et al. 2020). Teleost fishes have a high number of *aqp3*, *aqp7*, *aqp9*, and *aqp10* genes due to lineage- and species-specific gene duplications, whole-genome duplications, and deletions; their evolutionary history was described in detail by Yilmaz et al. (Yilmaz et al. 2020). The ancestral ray-finned fish acquired *aqp10.1* and *aqp10.2* through tandem duplication of *aqp10* (fig. 1*A*) and lost the *aqp13* gene. The former names of *aqp10.1* and *aqp10.2* are *aqp10a* (or *aqp10aa*) and *aqp10b* (or *aqp10ab*), respectively. In this article, gene symbols of tandem duplicates are appended with ".1" or ".2", whereas those of ohnologs, gene duplicates originating from genome duplication, are indicated by "a" or "b" following the Zebrafish Nomenclature Conventions (http://zfin.org/). Consequently, ancestral ray-finned fishes could have possessed five aquaglyceroporin genes: *aqp3*, *aqp7*, *aqp9*, *aqp10.1*, and *aqp10.2* (Yilmaz et al. 2020). In teleost fishes, these genes were doubled during the teleost-specific genome duplication (TGD), followed by lineage-specific gene losses or duplications (Yilmaz et al. 2020). Therefore, the number of paralogs, including ohnologs of aquaglyceroporin genes in teleosts, varies among species and lineages (Yilmaz et al. 2020). The majority of teleosts has one or two *aqp3* genes (*aqp3a* and *aqp3b*), whereas salmonids have a greater number of paralogs due to their lineage-specific tandem duplication (*aqp3a1a* and *aqp3a1b*) and whole-genome duplication (Yilmaz et al. 2020). Teleosts with a single *aqp3* gene usually retain *aqp3a* as opposed to *aqp3b*. Most teleosts possess one *aqp7* gene and two *aqp9* genes (*aqp9a* and *aqp9b*). The TGD resulted in *aqp10.1a* and *aqp10.1b* generated from the ancestral *aqp10.1* and *aqp10.2a* and *aqp10.2b* from the ancestral *aqp10.2* (fig. 1*A*). Note that the former names of *aqp10.1a*, *aqp10.1b*, *aqp10.2a*, and *aqp10.2b* are *aqp10aa*, *aqp10ba*, *aqp10ab*, and *aqp10bb*, respectively. After reciprocal genes losses from TGD-duplicated chromosomes, *aqp10.1a* and *aqp10.2b* genes are often retained on separate chromosomes, and most teleost species possess both *aqp10.1* and *aqp10.2*. *Polypterus* and *Lepisosteus*, so-called ancient ray-finned fishes, retained tandemly located *aqp10.1* and *aqp10.2* on the same chromosome, which suggest that ray-finned fishes require both *aqp10.1* and *aqp10.2*. Some teleost lineages, such as cod, have multiple *aqp10.1* genes (*aqp10.1a* and *aqp10.1b*), whereas others, such as herring, have multiple *aqp10.2* types (*aqp10.2a* and *aqp10.2b*) (fig. 1*B* and supplementary fig. S1, Supplementary Material online).

Recently, human (*Homo sapiens*) and Japanese pufferfish (*Takifugu rubripes*) Aqps (HsaAqps and TruAqps, respectively) were expressed in *Xenopus* oocytes and their water,

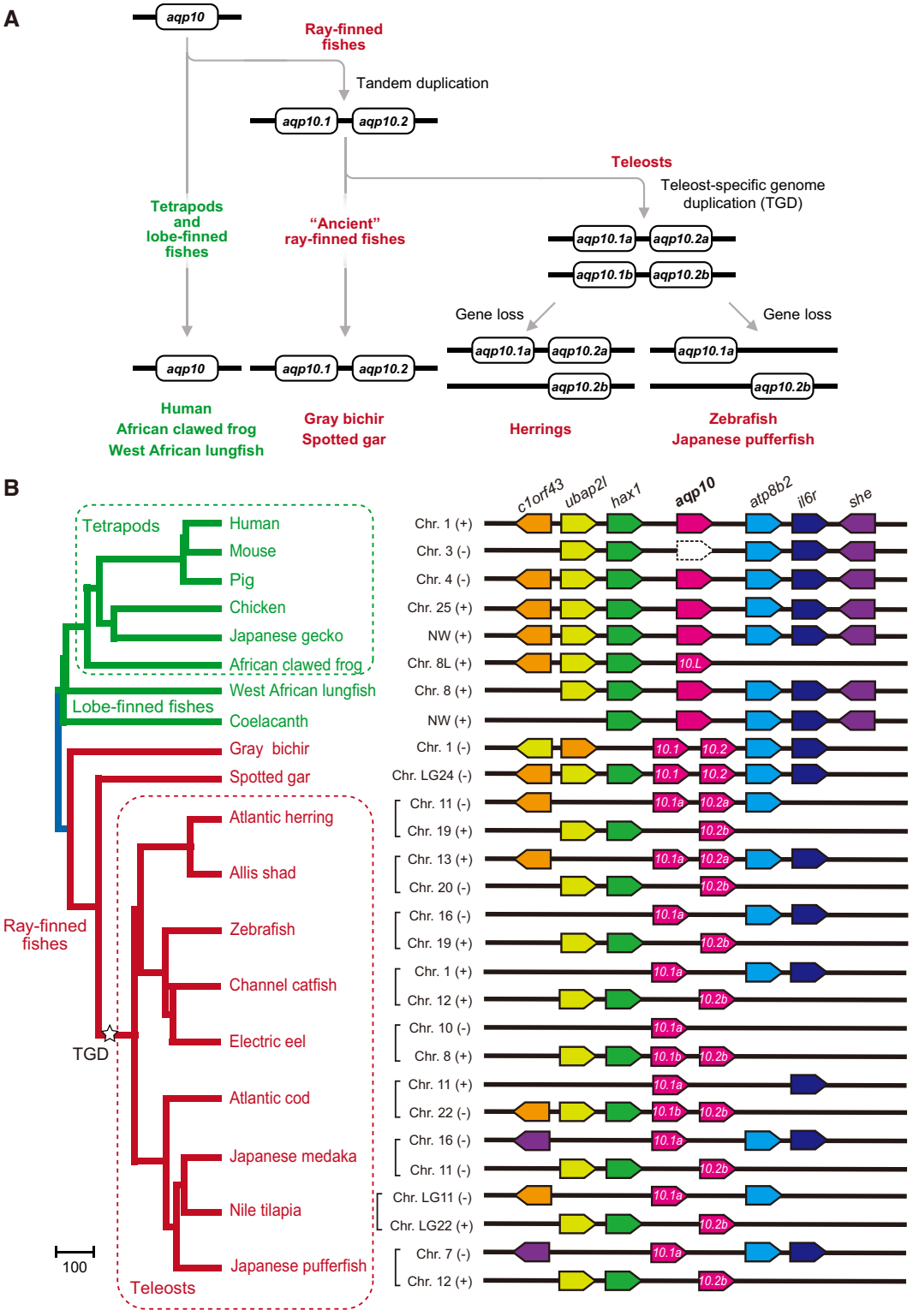

Fig. 1.—Evolutionary relationship of *aqp10* genes in the bony vertebrates analyzed in this study. (*A*) Flowchart showing how ray-finned fishes developed more than one *aqp10* gene through tandem gene duplication, TGD, and deletion (Yilmaz et al. 2020). (*B*) Synteny analyses of *aqp10* genes in bony vertebrates. (+) and (–) represent the right and left orientations, respectively, of the genome sequences in the NCBI and ENSEMBL databases. Synteny analysis was performed using the Ensembl genome browser (Martin et al. 2023) and NCBI genome viewer (Rangwala et al. 2021) with genome databases of various species (supplementary table S3, Supplementary Material online). Arrow-shaped boxes indicate the orientation of each gene. Dotted arrow-shaped boxes indicate pseudogenes. The phylogeny of bony vertebrate species based on the TimeTree database (http://www.timetree.org/) (Kumar et al. 2017) is shown on the left.

glycerol, urea, and boric acid permeabilities were analyzed (Ushio et al. 2022; Kumagai et al. 2023). The solute selectivity of the Aqp orthologs between humans and Japanese pufferfishes was similar, except for that of Aqp10; oocytes expressing HsaAqp10 were permeable to water, glycerol, urea, and boric acid, whereas those expressing TruAqp10.2b were permeable to water and glycerol but not to urea and boric acid. This difference in activity may have occurred after the two species diverged. These evolutionary adaptions in solute selectivity could present a promising model for analyzing the evolution of solute permeability in aquaglyceroporins. The plesiomorphic activities of Aqp10 and the evolutionary timing of changes in solute selectivity change during the evolution of bony vertebrates are unclear.

In this study, to elucidate the evolutionary history of solute selectivity of Aqp10, we analyzed and compared the permeability and evolutionary relationships of Aqp10s in eight bony vertebrate species: human, African clawed frog, West African lungfish, gray bichir, spotted gar, zebrafish, Pacific herring, and Japanese pufferfish. The results indicated that water, glycerol, urea, and boric acid permeabilities were plesiomorphic activities of Aqp10 and the ray-finned fish-specific paralog Aqp10.2 either lost or weakened urea and boric acid permeability from its common ancestor, that is to say, they may be novel examples of Aqp functional divergence by subfunction losses by one of the two duplicates.

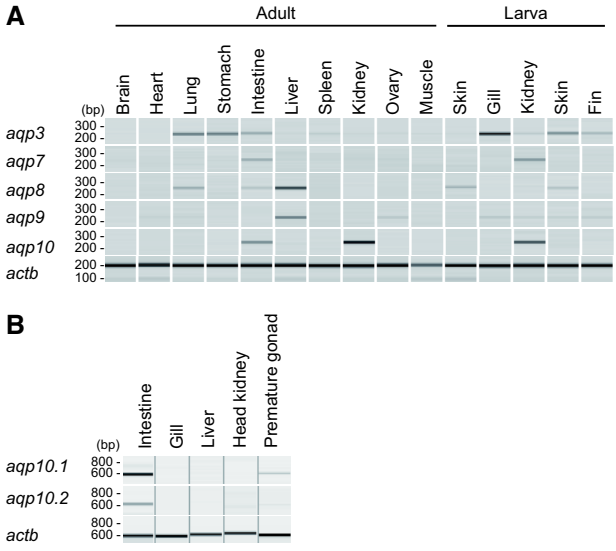

Fig. 2.—Tissue distribution of *aqp10s* in the African clawed frog (*A*) and spotted gar (*B*). (*A*) Expression profiles of *aqp10* and related aquaglyceroporin genes in African clawed frog tissues were determined using semiquantitative RT-PCR. Pseudo-gel images of the PCR products were generated using a microchip electrophoresis system. *actb* (β-actin gene) were used as an internal control. (*B*) Expression profiles of *aqp10.1* and *aqp10.2* in spotted gar tissues were determined using semiquantitative RT-PCR. *actb* was used as an internal control gene.

Results

Evolutional Relationships of the *aqp10* Genes in the Vertebrate Species

The evolutionary relationships of the *aqp10* paralogs used in the present study are summarized in fig. 1*A* according to the results of Yilmaz et al. (Yilmaz et al. 2020). We confirmed the evolutional relationship using phylogenetic and conserved synteny analyses (fig. 1*B*, supplementary fig. S1, Supplementary Material online) and that 1) tetrapods and lobe-finned fishes had a single *aqp10*; 2) a tandem gene duplication in ancestral ray-finned fishes (i.e., the common ancestor of *Polypterus*, *Lepisosteus*, and teleosts) generated *aqp10.1* and *aqp10.2*; 3) the TGD generated *aqp10.1a* and *aqp10.1b* from *aqp10.1* and *aqp10.2a* and *aqp10.2b* from *aqp10.2*, respectively, in ancestral teleost species; and 4) herring lost the *aqp10.1b* gene, whereas the Atlantic cod and electric eel lost *aqp10.2a* and the zebrafish and Japanese pufferfish lost both *aqp10.1b* and *aqp10.2a*.

Tissue Distribution of *aqp10s* in the African Clawed Frog and Spotted Gar

The expression distributions of *aqp10* in African clawed frog tissue and *aqp10.1* and aqp*10.2* in spotted gar were analyzed by semiquantitative reverse transcription polymerase chain reaction (RT-PCR). In addition, the tissue distributions of *aqp3*, *aqp7*, *aqp8*, and *aqp9* were investigated in the African clawed frog (fig. 2*A*). The expressions were as follows: *aqp10* was found in the intestines and kidneys primarily; *aqp3* in the lungs, stomach, intestine, liver, spleen, kidney, ovaries, skeletal muscle, skin, gills, and fins; *aqp7* in the intestine and larval kidneys; *aqp8* in the lungs, intestine, liver, and skin; and *aqp9* in the heart, lungs, liver, ovaries, skeletal muscles, gills, larval kidneys, larval skin, and fins. In spotted gar tissues, *aqp10.1* and *10.2* were highly expressed in the intestine (fig. 2*B*).

Solute and Water Permeability of Aqp10s in Tetrapods and a Lobe-Finned Fish

cRNAs for the Aqp10s of the African clawed frog (XlaAqp10) and West African lungfish (PanAqp10) were injected into *Xenopus* oocytes, and their solute and water permeabilities were analyzed using a swelling assay. For comparison, we also analyzed human Aqp10 (HsaAqp10). Oocytes expressing HsaAqp10, XlaAqp10, and PanAqp10 showed significant volume gains and increases in P_{water} in the hypo-osmotic solution (fig. 3, table 1), suggesting that these Aqp10s act as water channels in the plasma membranes of oocytes.

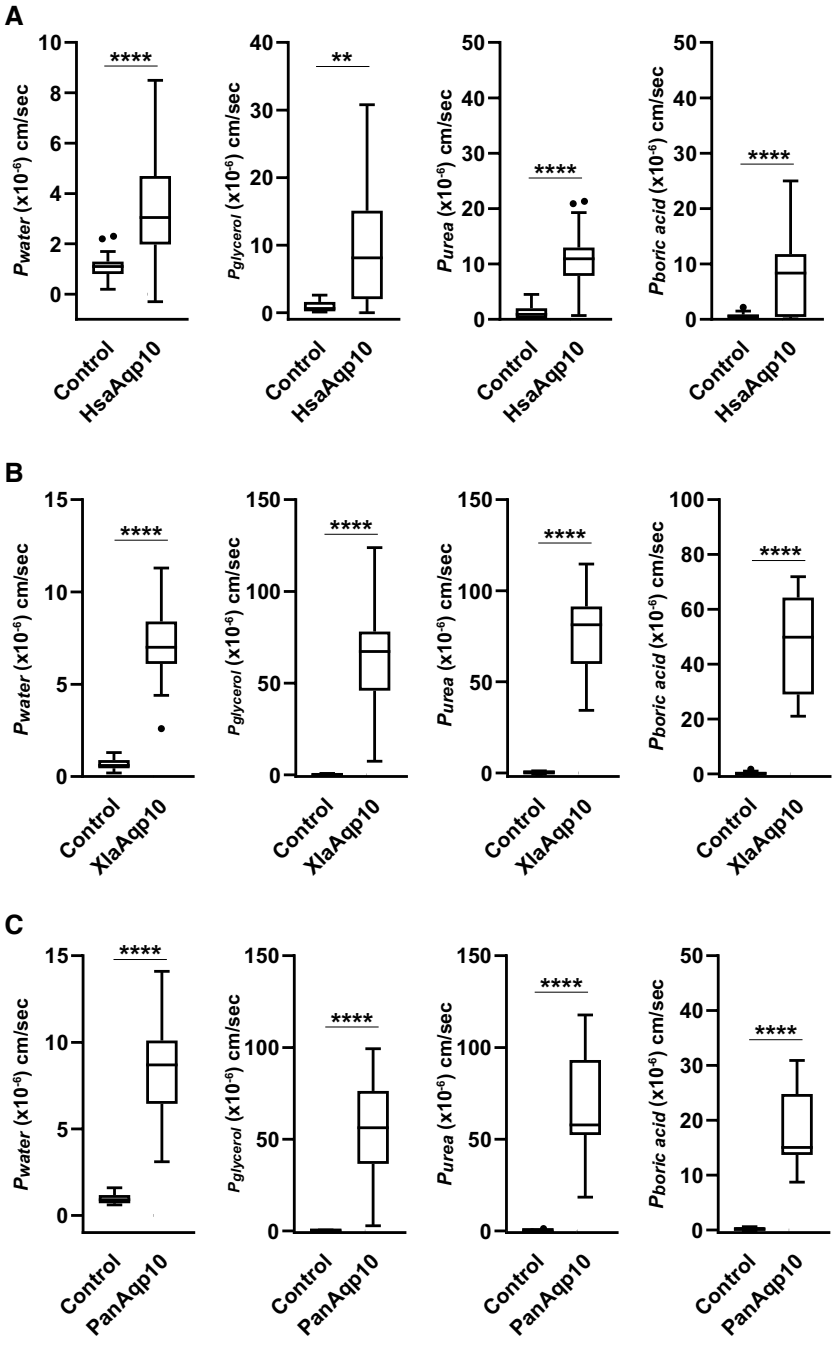

Fig. 3.—Water and solute (glycerol, urea, and boric acid) permeabilities of Aqp10s in humans (HsaAqp10) (*A*), African clawed frogs (XlaAqp10) (*B*), and West African lungfishes (PanAqp10) (*C*) as measured by a swelling assay. The change in the volume of oocytes expressing each Aqp10 was compared with that of control oocytes. Values are presented as interquartile ranges from the 25 to 75 percentile (box), range (whiskers), outliers (>1.5× the interquartile range above the upper quartile), and median (line in the box). Mean values, standard deviations, and total numbers of assayed oocytes are summarized in table 1. Statistical significance was evaluated by an unpaired *t*-test (****$P < 0.0001$; **$P < 0.01$).

The glycerol, urea, and boric acid permeabilities of oocytes expressing HsaAqp10, XlaAqp10, and PanAqp10 were analyzed by a swelling assay using an iso-osmotic solution containing 180 mM of glycerol, urea, or boric acid, respectively. Oocytes expressing HsaAqp10, XlaAqp10, and PanAqp10 showed significant volume gains and increases in $P_{glycerol}$, P_{urea}, and $P_{boric\ acid}$ (fig. 3, table 1), suggesting that these Aqp10s act as channels for all three compounds.

Table 1
Water and Solute Permeability Measurements of Aqp10s in Oocytes

Protein	P_{water} ($\times10^{-6}$ cm/s, 100 mosM Inside Osmotic Gradient)	$P_{glycerol}$ ($\times10^{-6}$ cm/s, 180 mM Outside Solute Gradient)	P_{urea} ($\times10^{-6}$ cm/s, 180 mM Outside Solute Gradient)	$P_{boric\ acid}$ ($\times10^{-6}$ cm/s, 180 mM Outside Solute Gradient)
HsaAqp10	3.3 ± 2.2 (30)	9.7 ± 8.7 (15)	10.7 ± 5.5 (22)	7.6 ± 6.6 (22)
Control1	1.1 ± 0.5 (27)	0.9 ± 0.9 (11)	1.1 ± 1.1 (24)	0.6 ± 0.5 (24)
XlaAqp10	7.4 ± 2.3 (15)	62.0 ± 27.7 (15)	78.5 ± 23.6 (15)	47.8 ± 17.5 (12)
Control2	0.7 ± 0.3 (13)	−0.1 ± 0.5 (13)	0.2 ± 0.7 (14)	0.2 ± 0.7 (11)
PanAqp10	8.2 ± 2.9 (16)	55.2 ± 27.4 (18)	68.1 ± 28.9 (18)	18.0 ± 6.7 (16)
Control3	1.0 ± 0.3 (16)	0.0 ± 0.3 (16)	0.0 ± 0.4 (15)	0.2 ± 0.3 (20)
TruAqp10.2b	5.7 ± 2.9 (10)	35.3 ± 21.1 (9)	2.1 ± 1.2 (10)	1.7 ± 0.6 (9)
Control4	1.5 ± 0.4 (10)	0.6 ± 1.1 (10)	1.1 ± 1.6 (10)	0.8 ± 0.7 (10)
DreAqp10.1a	12.3 ± 5.6 (9)	45.9 ± 26.6 (17)	79.7 ± 28.7 (11)	48.0 ± 23.6 (5)
DreAqp10.2b	6.6 ± 4.4 (9)	102.1 ± 25.2 (10)	12.0 ± 4.1 (14)	6.1 ± 3 (7)
Control5	0.8 ± 0.2 (9)	0.1 ± 0.4 (14)	0.2 ± 0.2 (14)	0.5 ± 0.4 (9)
CpaAqp10.1a	7.3 ± 2.8 (11)	72.7 ± 25.1 (6)	107 ± 41.1 (9)	70.9 ± 26.5 (13)
CpaAqp10.2a	5.9 ± 2.6 (10)	34.3 ± 13.6 (11)	31.5 ± 10.7 (7)	30.9 ± 15.8 (12)
CpaAqp10.2b	8.2 ± 5.6 (12)	131.2 ± 19 (4)	26.4 ± 3.8 (10)	16.0 ± 3.1 (11)
Control6	0.9 ± 0.3 (11)	0.0 ± 0.3 (11)	0.0 ± 0.4 (19)	0.2 ± 0.3 (24)
PseAqp10.1	10.0 ± 2.3 (10)	73.2 ± 32.8 (9)	85 ± 25.4 (7)	61.1 ± 27.8 (7)
PseAqp10.2	9.4 ± 4.6 (12)	79.6 ± 17.9 (7)	4.0 ± 0.7 (8)	2.8 ± 1.2 (7)
Control7	0.9 ± 0.3 (11)	0.0 ± 0.3 (11)	0.1 ± 0.5 (11)	0.1 ± 0.2 (16)
LocAqp10.1	7.2 ± 2.5 (11)	61.8 ± 25.9 (8)	104 ± 36 (10)	66.9 ± 28.4 (9)
LocAqp10.2	6.3 ± 2.2 (37)	46.1 ± 18.3 (40)	8.8 ± 3.3 (32)	4.1 ± 2 (37)
Control8	0.9 ± 0.3 (37)	0.2 ± 0.9 (35)	0.0 ± 0.4 (34)	0.2 ± 0.5 (36)

Values are presented as means ± standard deviations. Numbers in parentheses indicate the total number of oocytes assayed.

Solute and Water Permeability of Aqp10s of Teleost Species That Possess Two *aqp10* Paralogs, *aqp10.1a* and *aqp10.2b*

Zebrafishes and Japanese pufferfishes possess two *aqp10* paralogs, *aqp10.1a* and *aqp10.2b* (fig. 1), which is typical for teleosts (Yilmaz et al. 2020). The water permeabilities of zebrafish oocytes expressing Aqp10s (DreAqp10.1a and 10.2b) were analyzed using a swelling assay. In addition, we analyzed Japanese pufferfish Aqp10.2b (TruAqp10.2b) for comparison. We did not analyze TruAqp10.1a in this study because, in a previous study, TruAqp10.1a did not show activity when expressed in *Xenopus* oocytes for unknown reasons (Kumagai et al. 2023). Oocytes expressing Aqp10s showed significant volume gains and increases in P_{water} in the hypo-osmotic solution (fig. 4*A* and *B*, table 1), suggesting that these Aqp10s act as water channels in the plasma membrane of oocytes.

The glycerol, urea, and boric acid permeabilities of oocytes expressing TruAqp10.2b, DreAqp10.1a, and DreAqp10.2b were similarly analyzed using a swelling assay with an iso-osmotic solution containing the solutes. In the iso-osmotic solution containing glycerol, oocytes expressing TruAqp10.2b, DreAqp10.1a, and DreAqp10.2b showed significant volume gains and increases in $P_{glycerol}$ (fig. 4*A* and *B*, table 1), suggesting that these Aqp10s act as glycerol channels. In these experiments, the average $P_{glycerol}$ value for DreAqp10.2b was 2.2 times higher than that of DreAqp 10.1a, whereas the average P_{water} value for DreAqp10.2b was 1.9 times lower than that of DreAqp10.1a.

In the iso-osmotic solution containing urea or boric acid, DreAqp10.1a, but not DreAqp10.2b, showed significant volume gains and increases in P_{urea} and $P_{boric\ acid}$ (fig. 4*B*, table 1), suggesting that DreAqp10.1a, but not DreAqp10.2b, acts as a urea and boric acid channel. TruAqp10.2b showed a slight increase in $P_{boric\ acid}$ but no increase in P_{urea} (fig. 4*A*, table 1).

Solute and Water Permeability of Aqp10s of Teleost Species That Possess Three *aqp10* Paralogs, One *aqp10.1* and Two *aqp10.2* Ohnologs

Herring (Martinez Barrio et al. 2016) and shad (Sabatino et al. 2022) are unique in that they harbor one *aqp10.1* (*aqp10.1a*) and two *aqp10.2* s (*aqp10.2a* and *aqp10.2b*) (fig. 1) (Yilmaz et al. 2020); therefore, to understand the activity of Aqp10.2 ohnologs in teleosts, solute and water permeabilities of Aqp10s of Pacific herring (CpaAqp10.1a, 10.2a, and 10.2b) were analyzed by the *Xenopus* oocyte swelling assay. Oocytes expressing CpaAqp10s showed significant volume gains and increases in P_{water} in the hypo-osmotic solution (fig. 4*C*, table 1), suggesting that these Aqp10s act as water channels in the plasma membranes of oocytes.

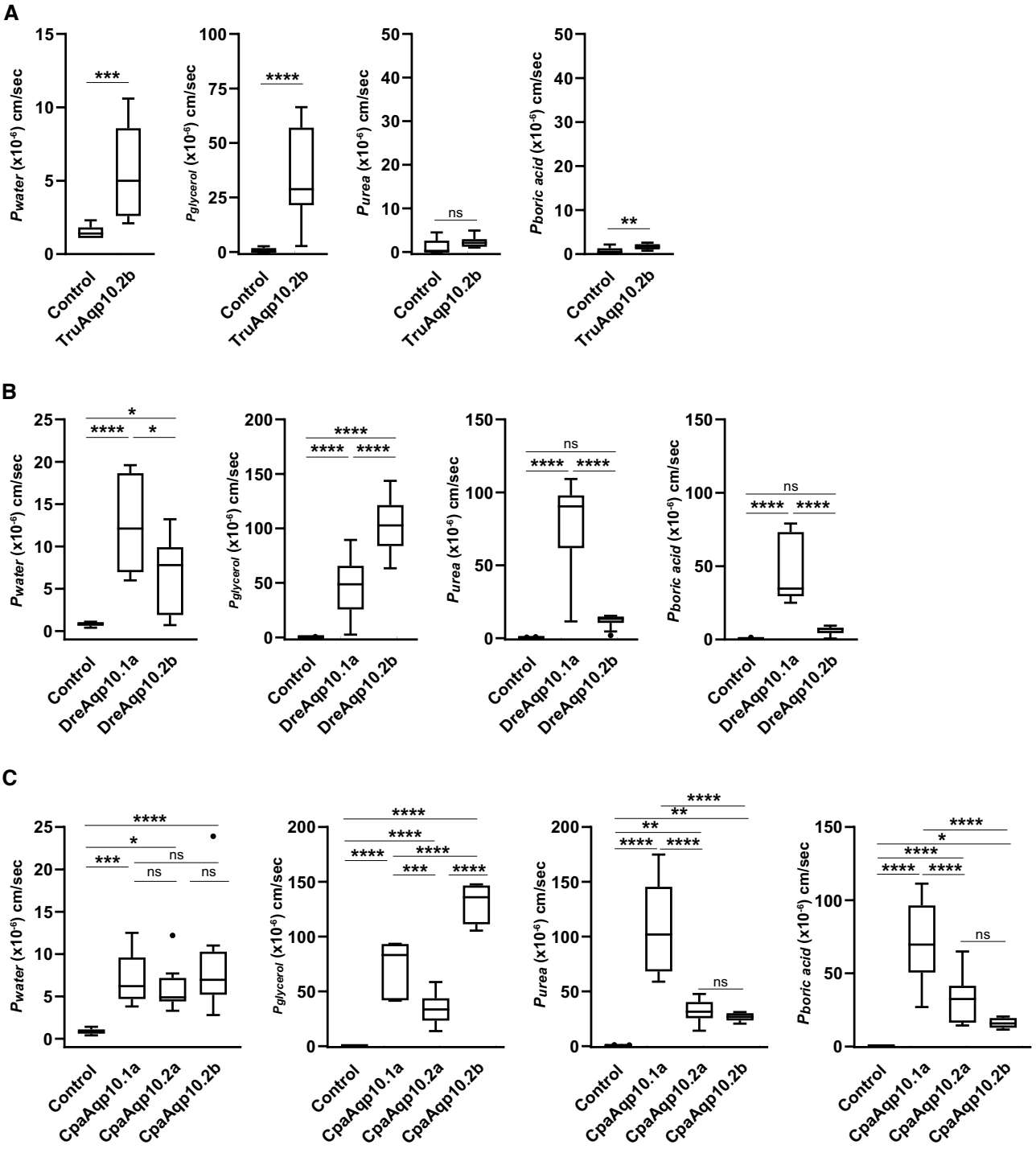

Fig. 4.—Water and solute (glycerol, urea, and boric acid) permeabilities of Aqp10*s* in Japanese pufferfishes (TruAqp10.2*b*) (*A*), zebrafishes (DreAqp10*s*) (*B*), and pacific herring (CpaAqp10*s*) (*C*) as measured by a swelling assay. The change in the volume of oocytes expressing each Aqp10 was compared with that of control oocytes. Values are presented as interquartile ranges from the 25 to75 percentiles (box), range (whiskers), outliers (>1.5× the interquartile range above the upper quartile), and median (line in the box). Mean values, standard deviations, and total numbers of assayed oocytes are summarized in table 1. Statistical significance for TruAqp10.2*b* was evaluated by an unpaired *t*-test (****$P < 0.0001$; ***$P < 0.001$). Statistical significance for DreAqp10*s* and CpaAqp10*s* was assessed by an ANOVA followed by Tukey's test (****$P < 0.0001$; ***$P < 0.001$; **$P < 0.01$; *$P < 0.05$).

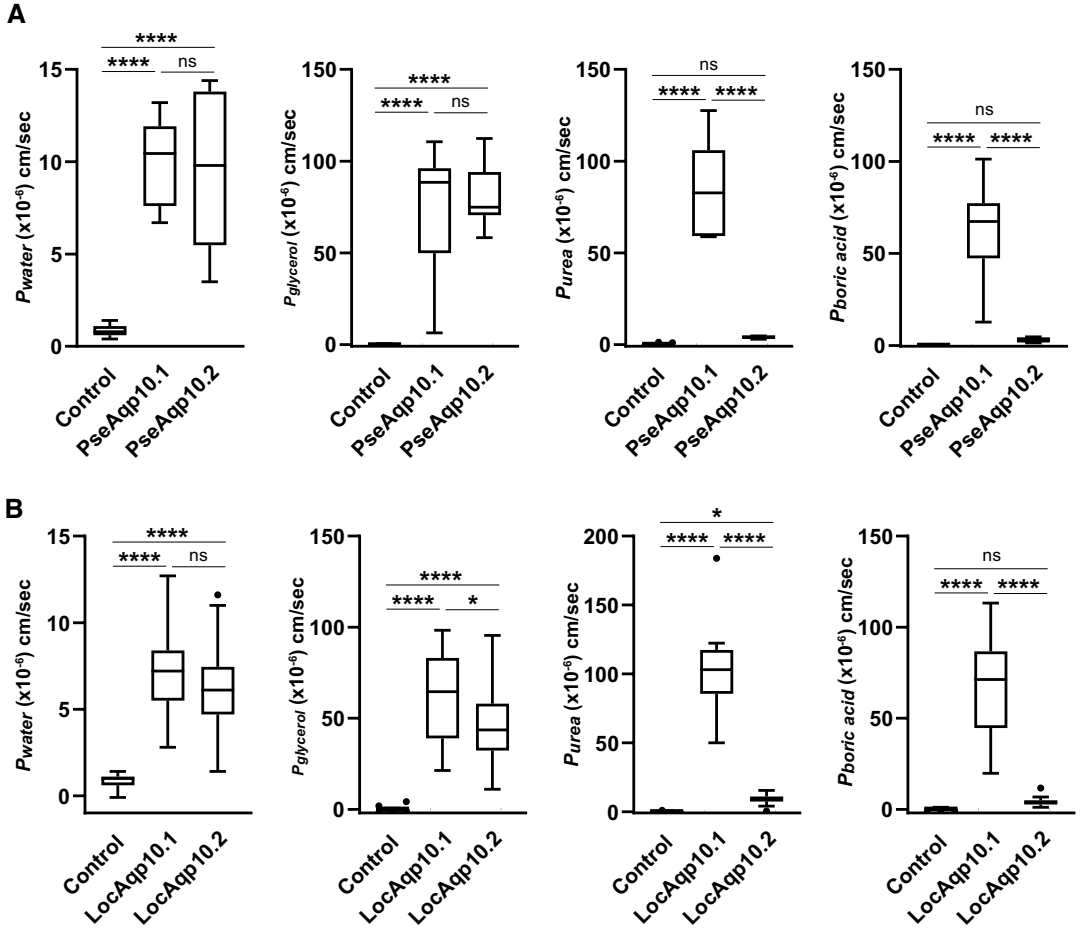

Fig. 5.—Water and solute (glycerol, urea, and boric acid) permeabilities of Aqp10*s* in gray bichirs (PseAqp10*s*) (*A*) and spotted gars (LocAqp10*s*) (*B*) as measured by a swelling assay. The change in the volume of oocytes expressing each Aqp10 was compared with that of control oocytes. Values are presented as interquartile ranges from the 25 to 75 percentiles (box), range (whiskers), outliers (>1.5× the interquartile range above the upper quartile), and median (line in the box). Mean values, standard deviations, and total numbers of assayed oocytes are summarized in table 1. Statistical significance was evaluated by an unpaired *t*-test (****$P < 0.0001$; *$P < 0.05$).

In the iso-osmotic solution containing glycerol, oocytes expressing CpaAqp10s showed significant volume gains and increases in $P_{glycerol}$ (fig. 4*C*, table 1), suggesting that these Aqp10s act as glycerol channels. In these experiments, the average values of $P_{glycerol}$ for CpaAqp10.1a and 10.2b were 2.1 and 3.8 times higher than those of CpaAqp10.2a, respectively, whereas the averages of P_{water} were not significantly different among the CpaAqp10s.

In the iso-osmotic solution containing urea and boric acid, oocytes expressing CpaAqp10.1a showed significant cell volume gains and increases in P_{urea} and $P_{boric\ acid}$ (fig. 4*C*, table 1), suggesting that CpaAqp10.1a acts as a urea and boric acid channel. CpaAqp10.2a and 10.2b showed a slight increase in P_{urea} and $P_{boric\ acid}$ (fig. 4*C*, table 1). However, in these experiments, the average values of P_{urea} and $P_{boric\ acid}$ of CpaAqp10.2a and 10.2b were 4.4–2.3 times lower than those of CpaAqp10.1a.

Solute and Water Permeability of *Xenopus* Oocytes Expressing Aqp10s of "Ancient" Ray-Finned Fishes

Gray bichir and spotted gar possess tandemly located *aqp10.1* and *aqp10.2* genes (fig. 1) (Yilmaz et al. 2020), and the Aqp10.1 and 10.2 of these species (PseAqp10s and LocAqp10s, respectively) were analyzed using a swelling assay. Oocytes expressing PseAqp10.1, PseAqp10.2, LocAqp10.1, and LocAqp10.2 showed significant volume gains and increases in P_{water} in the hypo-osmotic solution (fig. 5, table 1), suggesting that these Aqp10s act as water channels in the plasma membranes of oocytes.

The glycerol, urea, and boric acid permeabilities of oocytes expressing PseAqp10.1, PseAqp10.2, LocAqp10.1, and LocAqp10.2 were similarly analyzed by a swelling assay using an iso-osmotic solution containing solutes. Oocytes expressing PseAqp10s and LocAqp10s in the iso-osmotic solution containing glycerol showed significant volume

gains and increases in $P_{glycerol}$ (fig. 5, table 1), suggesting that these Aqp10s act as glycerol channels.

For the iso-osmotic solution containing urea or boric acid, PseAqp10.1 and LocAqp10.1, but not PseAqp10.2 and LocAqp10.2, showed significant volume gains and increases in P_{urea} and $P_{boric\ acid}$ (fig. 5, table 1), suggesting that PseAqp10.1 and LocAqp10.1, but not PseAqp10.2 and LocAqp10.2, act as urea and boric acid channels.

Discussion

The present study showed that Aqp10.2, which is an Aqp10 paralog of ray-finned fishes, has little or no urea nor boric acid transport activity and that these activities were systematically reduced and lost through evolution in the common ancestor of these fishes. According to Yilmaz et al. (Yilmaz et al. 2020), Aqp10 is widely expressed in cartilaginous fishes and bony vertebrates. Among the bony vertebrates, tetrapods and lobe-finned fishes have a single *aqp10*, whereas ray-finned fishes have two or more *aqp10* paralogs. Ancestors of ray-finned fishes acquired *aqp10.1* and *aqp10.2* through tandem duplication, and most extant species possess one or more genes derived from each of *aqp10.1* and *aqp10.2*. A previous study showed that human Aqp10 is permeable to water, glycerol, urea, and boric acid, whereas Japanese pufferfish Aqp10.2b, which is a paralog (e.g., ohnolog) of Aqp10.2, is permeable to water and glycerol, but not to urea or boric acid. In this study, we clarified the timing and history by which Aqp10 solute permeability evolved by analyzing the activity of 13 Aqp10s from eight bony vertebrate species.

The analysis of Aqp10 activity in an amphibian (the African clawed frog) and lobe-finned fish (the West African lungfish) showed permeability to water, glycerol, urea, and boric acid similar to that of human Aqp10, suggesting that solute selectivity is a common property of this protein in tetrapods and lobe-finned fishes (fig. 3). A subsequent analysis of Aqp10 activity of two zebrafish paralogs, Aqp10.1a and 10.2b, showed that Aqp10.1a was permeable to water, glycerol, urea, and boric acid, similar to human Aqp10. In contrast, Aqp10.2b was permeable to water and glycerol, but not to urea and boric acid, similar to the Japanese pufferfish Aqp10.2b (fig. 4*A* and *B*). This result indicates that urea and boric acid impermeability is a characteristic property of Aqp10.2b and is conserved among teleost species.

To determine when the Aqp10 solute selectivity changes occurred, we analyzed the Aqp10.1 and 10.2 functions in the "ancient" ray-finned fishes gray bichir and spotted gar (fig. 5). We found that Aqp10.1 was permeable to water, glycerol, urea, and boric acid in both species, similar to the Aqp10.1a in teleosts and the Aqp10s of tetrapods and lobe-finned fishes. Aqp10.2, however, was permeable to water and glycerol, but not to urea and boric acid, similar to Aqp10.2b in teleosts. These results strongly suggest that water, glycerol, urea, and boric acid permeabilities are plesiomorphic activities of Aqp10 that were retained by the Aqp10.1 of ray-finned fishes. In contrast, Aqp10.2 lost or weakened urea and boric acid permeabilities during evolution of the common ancestral species of ray-finned fishes.

To confirm whether the characteristics of Aqp10.2 were retained in both teleost-specific Aqp10 ohnologs, we used herring for our evaluation because these fishes retain *aqp10.2a* and *aqp10.2b*, whereas many teleosts only possess *aqp10.2b* (Yilmaz et al. 2020). The results indicated that CpaAqp10.1a increased P_{water}, $P_{glycerol}$, P_{urea}, and $P_{boric\ acid}$, whereas CpaAqp10.2a and 10.2b increased P_{water} and $P_{glycerol}$, and P_{urea} and $P_{boric\ acid}$ were much weaker than those of CpaAqp10.1a (fig. 4*C*). This result confirmed that Aqp10.2 in ancestral ray-finned species already had an absent or weakened urea and boric acid transport activity, and these characteristics were retained in teleost ohnologs. The presumed history of this lost or weakened urea and boric acid transport activity of teleost Aqp10.2 is illustrated in fig. 6.

Ray-finned fishes have both Aqp10.1 and 10.2; however, the physiological roles and reasons for retaining two types of Aqp10 with different solute permeabilities are not clear. So far, no reports have been identified that examine Aqp10 protein tissue localization in ray-finned fishes using immunohistochemistry, leaving the physiological functions of fish Aqp10s unclear, although the tissue distribution of Aqp10 in ray-finned fishes at the mRNA level has been reported in the zebrafish (Tingaud-Sequeira et al. 2010), Japanese pufferfish (Kumagai et al. 2023), Japanese eel (Kim et al. 2010), yellow croaker (Liu et al. 2019), and Atlantic salmon (Yilmaz et al. 2020). In the present study, we analyzed the distribution of Aqp10 mRNA in the spotted gar and found that both Aqp10.1 and Aqp10.2 were highly expressed in the intestine. Further analyses would be required to understand the roles of Aqp10.1 and 10.2 in ray-finned fishes.

Gene duplication is important for the distribution of multiple functions among duplicated genes. Redundant gene copies can be classified into four categories: neofunctionalization, subfunctionalization, gene conservation back-up compensation, and dosage amplification (Kuzmin et al. 2022). Neofunctionalization is defined as one of the duplicated genes maintaining the full function of the ancestral gene and the other acquiring a new function; thus, both genes are retained. Subfunctionalization is defined as the function of an ancestral gene being partitioned among duplicated genes. In this model, duplicated genes are retained because both are necessary to maintain the function or expression pattern of the protein (Hughes 1994; Force et al. 1999; Stoltzfus 1999). Indeed, gene duplication has been implicated in the evolution of the vertebrate Aqp superfamily, with the *aqp2*, *aqp5*, and *aqp6* clusters showing

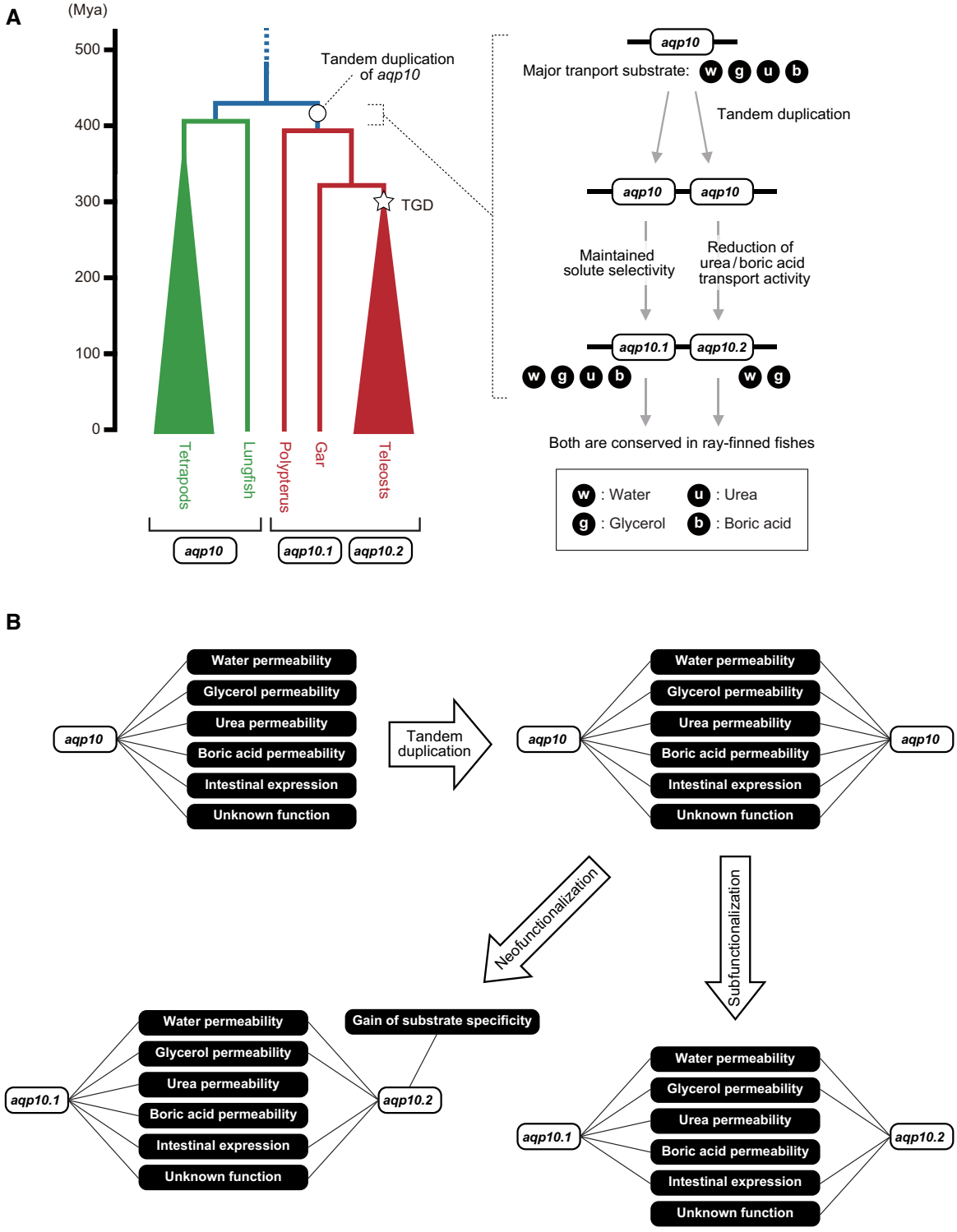

Fig. 6.—Evolutionary model and timing of *aqp10.1* and *aqp10.2* in ray-finned fishes. (*A*) The phylogeny of bony vertebrate species and time scale generated based on the TimeTree database (http://www.timetree.org/) (Kumar et al. 2017) is shown on the left. The right panel shows the hypothetical history of the method by which Aqp10.2 reduced or lost its urea and boric acid transport activity during evolution. TGD, teleost-specific genome duplication. (*B*) Evolutionary models of the functional divergence were illustrated by the model presented by He and Zhang (He and Zhang 2005).

different expression patterns in tetrapods as examples of subfunctionalization (Finn et al. 2014). As shown in this study, after tandem duplication, Aqp10.1 retained the full spectrum of plesiomorphic activities, whereas Aqp10.2 only retained water and glycerol permeabilities but lost urea and boric acid permeabilities. Although we do not have evidence for either of the two tandem duplicates acquiring a novel functionality, Aqp10.2 secondarily lost some of the ancestral subfunctions. Therefore, although we do not see a reciprocal loss of subfunctions for the Aqp10.1 paralog, the functional divergence of Aqp10 paralogs is most consistent with a subfunctionalization/functional specialization mechanism.

More specifically, what mechanism, then, could be responsible for the weakening of the urea and boric acid permeabilities of Aqp10.2? We propose two possibilities: 1) Aqp10.2 lost the structure necessary for urea and boric acid transport, or 2) Aqp10.2 acquired a filter that distinguishes urea and boric acid from glycerol and restricting urea and boric acid transport. In case 1), Aqp10.2 would be considered a type of subfunctionalization because it lost some functions of the ancestral gene and maintained some of them (fig. 6*B*) (He and Zhang 2005), and Aqp10.1 could potentially have lost some of the unknown functions of the ancestral gene. In case 2), Aqp10.2 retained some functions of the ancestral gene and gained a novel function, solute selectivity, and could be considered neofunctionalization (fig. 6*B*). Although the current data are more consistent with the subfunctionalization model due to loss of subfunctions for Aqp10.2, we cannot exclude the possibility of neofunctionalization by gain of novel solute selectivity in Aqp10.2 and hence functional specialization hidden as subfunction partitioning.

Structurally, water-specific Aqps have selective filters that block the permeability of molecules other than water (Hub and de Groot 2008; Gotfryd et al. 2018). The Asn-Pro- Ala (NPA) motif and the aromatic/Arg (ar/R) selectivity filter modulate the transport substrate specificity of Aqps. However, the mechanisms underlying solute selectivity among aquaglyceroporins have not been well studied. Kitchen et al. reported that human Aqp3 is highly permeable to glycerol but not to urea and that site-directed mutagenesis of human Aqp3, in which tyrosine 212 was mutated to alanine (Y212A), increases the urea permeability without affecting glycerol permeability (Kitchen et al. 2019). Therefore, Y212 is involved in the restriction of urea permeability in human Aqp3. However, Aqp10 of the African clawed frog, despite having a tyrosine residue at the same sites (supplementary fig. S2, Supplementary Material online), exhibits urea permeability (fig. 3). This result suggests that tyrosine residues may not solely contribute to the restriction of urea permeability in Aqp10. Kitchen et al. also stated that pore size is insufficient to explain the solute selectivity of Aqps and that the substrate discrimination in Aqps depends on a complex interplay between 1) the actual residues forming the ar/R region, 2) the physical size and chemical properties of the filter created by these residues, and 3) the structural context in which they are situated (Kitchen et al. 2019). Therefore, the question of how the Aqp10.2 of ray-finned fishes lost its urea and boric acid transport activity is critical. Because the solute selectivities of Aqp10, Aqp10.1, and Aqp10.2 have been characterized in this study, it is expected that a more detailed mechanism that influences the solute selectivity should and will be elucidated by future investigations. These future, mechanistic studies should lead to the determination of which model, subfunctionalization or neofunctionalization, is more consistent with the pleiotropy identified here.

Materials and Methods

Semiquantitative RT-PCR

Previously prepared total RNAs (Tran et al. 2006; Motoshima et al. 2023) were used in this study. First-strand complementary DNA was synthesized from 5 μg of total RNA using the SuperScript IV First-Strand Synthesis System (Thermo Fisher Scientific, Waltham, MA, USA) with oligo(dT) primers and analyzed by RT-PCR, as described previously (Tran et al. 2006; Motoshima et al. 2023). The cDNA was diluted 8-fold with nuclease-free water and used as a template for PCR with gene-specific primers (supplementary table S1, Supplementary Material online). Each reaction mixture (final volume, 12.5 μL) consisted of 0.25 μL cDNA (template), primers (individual final concentration, 0.25 μM), and 6.25 μL GoTaq Green Master Mix (2×; Promega, Madison, WI, USA).

The PCR conditions were as follows: initial denaturation at 94 °C for 2 min; 28 cycles (African clawed frog *aqp3*, *7*, *8*, *9*, *10*, and *actb*; spotted gar *aqp10s* and *actb*) of 94 °C for 15 s (denaturation); 52 °C (African clawed frog *aqp7*, *8*, *9*, *10*, and *actb*), 54 °C (African clawed frog *aqp3*), or 55 °C (spotted gar *aqp10s* and *actb*) for 30 s (annealing); 72 °C for 1 min (extension); and a final extension at 72 °C for 7 min. After amplification, 3 μL of the PCR mixture was diluted and loaded onto a microchip electrophoresis system for DNA/RNA analysis (MCE-202 MultiNA, Shimadzu, Kyoto, Japan) using a DNA-12000 reagent kit (Shimadzu) according to the manufacturer's instructions. Electrophoresis results were analyzed using the MultiNA Viewer software (Shimadzu).

Cloning of Aqp10s from the African Clawed Frog, West African Lungfish, Gray Bichir, Spotted Gar, Zebrafish, and Pacific Herring

All animal protocols and procedures were conducted in accordance with the National Institutes of Health "Guide for the Care and Use of Laboratory Animals" and in accordance with a manual approved by the Institutional Animal Experiment Committee of the Tokyo Institute of

Technology. Pacific herring were quickly decapitated, and intestinal tissues were dissected and stored in RNAlater solution (Thermo Fisher Scientific). We used Pacific herring but not Atlantic herring for cDNA cloning, because fresh tissues of Atlantic herring were not available in Japan. Total RNAs were isolated from the Pacific herring intestines using the acid guanidinium thiocyanate–phenol–chloroform extraction method with Isogen (Nippon Gene, Tokyo, Japan). The concentration and quality of the RNA were measured based on the UV absorbance at 260 and 280 nm and checked using the MultiNA and an RNA reagent kit (Shimadzu). First-strand complementary DNA was synthesized as described above and used to obtain full-length cDNAs of Aqp10s from the Pacific herring.

Full-length cDNAs of Aqp10s from the African clawed frog, spotted gar, and zebrafish were isolated from previously prepared intestinal cDNA of each species (Tran et al. 2006; Motoshima et al. 2023). Full-length cDNAs of Aqp10s from the West African lungfish and gray bichir Aqp10s were chemically synthesized (Eurofins Genomics, Tokyo, Japan).

cDNAs were amplified by PCR using a high-fidelity DNA polymerase (KOD-Plus-Neo or KOD One PCR Master Mix, Toyobo, Osaka, Japan), and primers were designed based on the genomic database of African clawed frog (*Xenopus laevis*, GCF_017654675.1) (Session et al. 2016), West African lungfish (*Protopterus annectens*, GCF_019279795.1) (Wang et al. 2021), Gray bichir (*Polypterus senegalus*, GCF_016835505.1) (Bi et al. 2021), Spotted gar (*Lepisosteus oculatus*, GCF_000242695.1) (Braasch et al. 2016), Zebrafish (*Danio rerio*, GCF_000002035.6) (Howe et al. 2013), Atlantic herring (*Clupea harengus*, GCF_900700415.2) (Martinez Barrio et al. 2016), (supplementary table S1, Supplementary Material online). cDNAs were subcloned into pGEMHE (Liman et al. 1992) with the In-Fusion Snap Assembly Master Mix (Takara Bio, Shiga, Japan) using gene-specific primers with 15 bp sequences complementary to the ends of the linearized pGEMHE (supplementary table S1, Supplementary Material online) and then sequenced. The newly identified sequences were deposited under their respective GenBank/EMBL/DDBJ accession numbers (spotted gar LocAqp10.1, LC767942, and LocAqp10.2, LC767946; Pacific herring CpaAqp10.1a, LC767943, CpaAqp10.2a, LC767944, and CpaAqp10.2b, LC767945). The sequences of African clawed frog XlaAqp10, West African lungfish PanAqp10, gray bichir PseAqp10.1 and 10.2, and zebrafish DreAqp10.1a and 10.2b were confirmed to be identical to those reported or predicted (XP_041429683.1, XP_043936577.1, XP_039607769.1, XP_039607747.1, NP_001002349, and XP_005159449, respectively).

Expression of Aqp10s in *Xenopus* Oocytes

In addition to the expression vectors described above, we used previously prepared vectors for human Aqp10 (HsaAqp10) and Japanese pufferfish Aqp10.2b (TruAqp10.2b) as references (Ushio et al. 2022; Kumagai et al. 2023). The plasmids were linearized with NotI and capped RNAs (cRNAs) were transcribed in vitro using the T7 mMessage mMachine kit (Thermo Fisher Scientific). For PanAqp10, cRNA was transcribed in vitro using the T7 mMessage mMachine Ultra Kit (Thermo Fisher Scientific).

Xenopus laevis oocytes were dissociated with collagenase as described previously (Romero et al. 1998; Ushio et al. 2022; Kumagai et al. 2023) and injected with 50 nL of water or a solution containing 0.5 ng/nL cRNA (25 ng/oocyte), using a Nanoject II injector (Drummond Scientific, Broomall, PA, USA). Oocytes were incubated at 16 °C in OR3 medium and observed for 3–5 days after injection. The OR3 medium (1 L) consisted of 0.7% *w/v* powdered Leibovitz L-15 medium with L-glutamine (Thermo Fisher Scientific), 50 mL of 10,000 U penicillin, 10,000 U streptomycin solution in 0.9% NaCl (Sigma-Aldrich, St Louis, MO, USA), and 5 mM HEPES (pH 7.50). The osmolality was adjusted to 200 mOsmol/kg with NaCl powder (Romero et al. 1998; Ushio et al. 2022; Kumagai et al. 2023). The frogs were handled and the oocytes harvested according to the approved protocol described in the previous section.

Swelling Assay

Oocyte swelling was monitored using a stereomicroscope (SZX9; Olympus, Tokyo, Japan) equipped with a charge-coupled device (CCD) camera (DS-Fi2; Nikon, Tokyo, Japan) as described previously (Ushio et al. 2022; Kumagai et al. 2023). The oocyte volumes were calculated assuming spherical geometry. Oocytes incubated with ND96 (~200 mOsmol/kg) were transferred to 2-fold diluted ND96 (~100 mOsmol/kg) for the water transport assays. For the glycerol, urea, and boric acid transport assays, oocytes were transferred to an isotonic solution containing ND96 supplemented with 180 mM glycerol, urea, or boric acid instead of NaCl and adjusted to an osmolality of ~200 mOsmol/kg.

Water permeability (P_{water}) was calculated from the osmotic swelling data and the molar volume of water ($V_w = 18\ cm^3/mol$) as follows (Preston et al. 1992): $P_{water} = [V_o \times d(V/V_o)/dt]/[S \times V_w \times (osm_{in} - osm_{out})]$, where S is the initial oocyte surface area. Solute permeability (P_{solute}) was calculated from the swelling data, total osmolality of the system ($osm_{total} = 200$ mOsmol/kg), and solute gradient ($sol_{out} - sol_{in}$) as follows (Carbrey et al. 2003): $P_{solute} = osm_{total} \times [V_o \times d(V/V_o)/dt]/[S \times (sol_{out} - sol_{in})]$.

The water, glycerol, urea, and boric acid transport activities of each Aqp10 were evaluated using oocytes from the same animal, and the experiment was repeated using a minimum of three frogs. Quantitative data are presented as mean ± standard deviation (SD) in table 1. P_{water} and P_{solute} values were compared among oocytes expressing

Aqp10s and control oocytes, and the statistical significance for species with only one Aqp10 (human, African clawed frog, West African lungfish, and Japanese pufferfish) was evaluated using an unpaired *t*-test. For species with two or more Aqp10 paralogs, statistical significance was assessed using a one-way analysis of variance (ANOVA), followed by Tukey's test, using GraphPad Prism software (version 5, GraphPad, San Diego, CA, USA). This software was also used to display the results in box plots.

Supplementary Material

Supplementary data are available at *Genome Biology and Evolution* online (http://www.gbe.oxfordjournals.org/).

Acknowledgments

We thank Takeshi Furukawa (Executive Director, AMF), Makoto Kuraishi, Toshiaki Mori, Rintaro Ishii, and Mai Hibino for capture and husbandry of Pacific herring; Brett Racicot for gar husbandry; and Shin-ichiro Hidaka, Natsue Yamamoto, Michiko Kotani, Tomoko Narisawa, Sachiko Muto, Satomi Asano, Yoko Yamamoto, Nana Shinohara, Atsumi Sakaguchi, the Biomaterials Analysis Division, and the Open Research Facilities for Life Science and Technology at the Tokyo Institute of Technology for their technical assistance. This study was supported by Japan Society for the Promotion of Science (grant numbers 17H03870, 21H02281, 21K14781, and 19H03272). Gar work in the Braasch Lab is supported by NSF EDGE grant #2029216. The Romero laboratory work was supported by NIH RO1 DK092408, NIH U54 DK100227, and the Mayo Foundation.

Author Contributions

G.I., K.U., A.K., and A.N. conceived and designed the research; G.I., K.U., I.B., E.W., S.K., K.M., A.K., and A.N. performed the experiments; G.I., K.U., H.N., T.F., A.K., and A.N. analyzed the data; G.I., K.U., H.N., I.B., T.F., M.F.R., A.K., and A.N. interpreted the results of the experiments; G.I., K.U., A.K., and A.N. prepared the figures; G.I., K.U., A.K., and A.N. drafted the manuscript; H.N., I.B., T.F., M.F.R., A.K., and A.N. edited and revised the manuscript; and G.I., K.U., H.N., I.B., E.W., S.K., T.F., K.M., M.F.R., A.K., and A.N. approved the final version of the manuscript.

Data Availability

The data underlying this article are available in GenBank under accession numbers indicated in Materials and Methods.

Literature Cited

Agre P, et al. 2002. Aquaporin water channels–from atomic structure to clinical medicine. J Physiol. 542:3–16.

Azad AK, et al. 2021. Human aquaporins: functional diversity and potential roles in infectious and non-infectious diseases. Front Genet. 12:654865.

Bi X, et al. 2021. Tracing the genetic footprints of vertebrate landing in non-teleost ray-finned fishes. Cell 184:1377–1391.e1314.

Borgnia M, Nielsen S, Engel A, Agre P. 1999. Cellular and molecular biology of the aquaporin water channels. Ann Rev Biochem. 68: 425–458.

Braasch I, et al. 2016. The spotted gar genome illuminates vertebrate evolution and facilitates human-teleost comparisons. Nat Genet. 48:427–437.

Calamita G, Delporte C. 2021. Involvement of aquaglyceroporins in energy metabolism in health and disease. Biochimie 188:20–34.

Carbrey JM, et al. 2003. Aquaglyceroporin AQP9: solute permeation and metabolic control of expression in liver. Proc Natl Acad Sci U S A. 100:2945–2950.

Chauvigne F, et al. 2019. The vertebrate Aqp14 water channel is a neuropeptide-regulated polytransporter. Commun Biol. 2:462.

Finn RN, Cerda J. 2015. Evolution and functional diversity of aquaporins. Biol Bull. 229:6–23.

Finn RN, Chauvigne F, Hlidberg JB, Cutler CP, Cerda J. 2014. The lineage-specific evolution of aquaporin gene clusters facilitated tetrapod terrestrial adaptation. PLoS One 9:e113686.

Force A, et al. 1999. Preservation of duplicate genes by complementary, degenerative mutations. Genetics 151:1531–1545.

Gotfryd K, et al. 2018. Human adipose glycerol flux is regulated by a pH gate in AQP10. Nat Commun. 9:4749.

Hara-Chikuma M, Verkman AS. 2008. Roles of aquaporin-3 in the epidermis. J Invest Dermatol. 128:2145–2151.

He X, Zhang J. 2005. Rapid subfunctionalization accompanied by prolonged and substantial neofunctionalization in duplicate gene evolution. Genetics 169:1157–1164.

Howe K, et al. 2013. The zebrafish reference genome sequence and its relationship to the human genome. Nature 496:498–503.

Hub JS, de Groot BL. 2008. Mechanism of selectivity in aquaporins and aquaglyceroporins. Proc Natl Acad Sci U S A. 105: 1198–1203.

Hughes AL. 1994. The evolution of functionally novel proteins after gene duplication. Proc Biol Sci. 256:119–124.

Kim YK, Watanabe S, Kaneko T, Huh MD, Park SI. 2010. Expression of aquaporins 3, 8 and 10 in the intestines of freshwater-and seawater-acclimated Japanese eels *Anguilla japonica*. Fish Sci. 76:695–702.

Kitchen P, et al. 2019. Water channel pore size determines exclusion properties but not solute selectivity. Sci Rep. 9:20369.

Kumagai S, et al. 2023. Boric acid transport activity of marine teleost aquaporins expressed in Xenopus oocytes. Physiol Rep. 11: e15655.

Kumar S, Stecher G, Suleski M, Hedges SB. 2017. TimeTree: a resource for timelines, timetrees, and divergence times. Mol Biol Evol. 34: 1812–1819.

Kuzmin E, Taylor JS, Boone C. 2022. Retention of duplicated genes in evolution. Trends Genet. 38:59–72.

Laforenza U, Bottino C, Gastaldi G. 2016. Mammalian aquaglyceroporin function in metabolism. Biochim Biophys Acta. 1858:1–11.

Lebeck J. 2014. Metabolic impact of the glycerol channels AQP7 and AQP9 in adipose tissue and liver. J Mol Endocrinol. 52: R165–R178.

Liman ER, Tytgat J, Hess P. 1992. Subunit stoichiometry of a mammalian K^+ channel determined by construction of multimeric cDNAs. Neuron 9:861–871.

Liu C, et al. 2019. Low temperature-induced variation in plasma biochemical indices and aquaglyceroporin gene expression in the large yellow croaker *Larimichthys crocea*. Sci Rep. 9:2717.

Martin FJ, et al. 2023. Ensembl 2023. Nucleic Acids Res. 51: D933–D941.
Martinez Barrio A, et al. 2016. The genetic basis for ecological adaptation of the Atlantic herring revealed by genome sequencing. eLife 5:e12081.
Matsumura K, et al. 2007. Aquaporin 7 is a beta-cell protein and regulator of intraislet glycerol content and glycerol kinase activity, beta-cell mass, and insulin production and secretion. Mol Cell Biol. 27: 6026–6037.
Morinaga T, Nakakoshi M, Hirao A, Imai M, Ishibashi K. 2002. Mouse aquaporin 10 gene (AQP10) is a pseudogene. Biochem Biophys Res Commun. 294:630–634.
Motoshima T, et al. 2023. Na^+-Cl^- cotransporter 2 is not fish-specific and is widely found in amphibians, non-avian reptiles, and select mammals. Physiol Genomics. 55:113–131
Preston GM, Carroll TP, Guggino WB, Agre P. 1992. Appearance of water channels in *Xenopus* oocytes expressing red cell CHIP28 protein. Science 256:385–387.
Rangwala SH, et al. 2021. Accessing NCBI data using the NCBI sequence viewer and genome data viewer (GDV). Genome Res. 31:159–169.
Romero MF, Fong P, Berger UV, Hediger MA, Boron WF. 1998. Cloning and functional expression of rNBC, an electrogenic Na^+-HCO_3^- cotransporter from rat kidney. Am J Physiol. 274:F425–F432.
Sabatino SJ, et al. 2022. The genetics of adaptation in freshwater Eurasian shad (Alosa). Ecol Evol. 12:e8908.
Session AM, et al. 2016. Genome evolution in the allotetraploid frog *Xenopus laevis*. Nature 538:336–343.
Stoltzfus A. 1999. On the possibility of constructive neutral evolution. J Mol Evol. 49:169–181.
Tanaka Y, Morishita Y, Ishibashi K. 2015. Aquaporin10 is a pseudogene in cattle and their relatives. Biochem Biophys Rep. 1:16–21.
Tingaud-Sequeira A, et al. 2010. The zebrafish genome encodes the largest vertebrate repertoire of functional aquaporins with dual paralogy and substrate specificities similar to mammals. BMC Evol Biol. 10:38.
Tran YH, et al. 2006. Spliced isoforms of LIM-domain-binding protein (CLIM/NLI/Ldb) lacking the LIM-interaction domain. J Biochem. 140:105–119.
Ushio K, et al. 2022. Boric acid transport activity of human aquaporins expressed in *Xenopus* oocytes. Physiol Rep. 10:e15164.
Wang K, et al. 2021. African lungfish genome sheds light on the vertebrate water-to-land transition. Cell 184:1362–1376.e1318.
Yilmaz O, et al. 2020. Unravelling the complex duplication history of deuterostome glycerol transporters. Cells 9:1663.

Associate editor: Yoko Satta

Supplementary Table S1. List of primers used for polymerase chain reaction amplification of Aqp10s in bony vertebrates

Species	Gene	Accession	Remarks	Direction	Sequence (5' to 3')
African clawed frog	*aqp10.L*	XM_041573749.1	RT-PCR	Fw	GTCACCTGAACCCTGCCTAC
				Rv	ACGCTGTCTCTCTAGGTCCA
			Full-length cDNA	Fw	ATGCCCAGGCTTTATATAAGGAGCA
				Rv	TCACAGGCGGTGGGAGAG
			In-Fusion cloning	Fw	gcagatcattccccATGCTAGGAATGCCTAGACTTTATAT
				Rv	agaattcggatcccTCACAGACGGTGGGAGAGGGGATT
Spotted gar	*aqp10.1*	LC767942	RT-PCR	Fw	GCTGGCGATTCGGAACCA
				Rv	CTGTTGAGCCTGTCGTCCAA
			Full-length cDNA	Fw	ATGGAGAAGGTGAAGCGCGTGCTG
				Rv	*TCAGGGGTCCCAGCTGGGCATGG*
			In-Fusion cloning	Fw	gcagatcaattccccATGGAGAAGGTGAAGCGCG
				Rv	agaattcggatcccTCAGGGGTCCCAGCTGG
Spotted gar	*aqp10.2*	XM_015368732.1 LC767946	RT-PCR	Fw	ACAGAGACTGTTCCAGGTACA
				Rv	CATCACCCAGAGCCAGAACA
			Full-length cDNA	Fw	ATGGAGAAGGTACAGAGACTGTTCCAGGTACAGAA
				Rv	ATAGAGCTCTTCCCTGTGGCAGGTGTTTCCCGTTG
			In-Fusion cloning	Fw	gcagatcaattccccaATGGAGAAGGTACAGAGACTG
				Rv	agaattcggatcccTCAGAGGCGGTGGGTGAC
Zebrafish	*aqp10.1a*	NM_001002349.1	Full-length cDNA	Fw	ATGAAGAGGATGAAGGTGAAAAATGAACTGGCACG
				Rv	ttccagactttTTAAATTGAAGACATTTTAAGG
			In-Fusion cloning	Fw	gcagatcaattccccaATGAAGAGGATGAAGGTGAAAAATG
				Rv	agaattcggatcccTTAAATTGAAGACATTTTAAGG
Zebrafish	*aqp10.2b*	XM_005159392.4	Full-length cDNA	Fw	ATGGACCGTCTGCTGAGGA
				Rv	TTACCCTACGTCTGCTGAGGTTAT
			In-Fusion cloning	Fw	gcagatcattccccATGGACCGTCTGCTGAGGAGATAC
				Rv	agaattcggatcccTTACCCTACGTCTGCTGAGGTTATAG
Pacific herring	*aqp10.1a*	LC767943	Full-length cDNA	Fw	TTGACCGGCAGAATGAAGCAGGTGAG
				Rv	CTATAGGTTCGTTCCTTTAATGATTGTCG
			In-Fusion cloning	Fw	gcagatcattccccTTGACCGGCAGAATGAAGC
				Rv	agaattcggatcccCTATAGGTTCGTTCCTTTAA
Pacific herring	*aqp10.2a*	LC767944	Full-length cDNA	Fw	ATGGAAAGAGCACGAGGACTATGC
				Rv	TCACACATTGTCCAAATTCTCATCC
			In-Fusion cloning	Fw	gcagatcattccccATGGAAAGAGCACGAGGAC
				Rv	agaattcggatcccTCACACATTGTCCAAATTC
Pacific herring	*aqp10.2b*	LC767945	Full-length cDNA	Fw	ATGGATCGGCTTTTAAGGAGGTGTC
				Rv	TCATTGCCCCCAGAGGCTGTGCACT
			In-Fusion cloning	Fw	gcagatcattccccATGGATCGGCTTTTAAGGAG
				Rv	agaattcggatcccTCATTGCCCCCAGAGGCTG
West African lungfish	*aqp10*	XM_044080642.1	In-Fusion cloning	Fw	gcagatcattccccATGCTTTCATACCCACCACA
				Rv	agaattcggatcccCTAAGTACCCATTATTATGT
Gray bichir	*aqp10.1*	XM_039751835.1	In-Fusion cloning	Fw	gcagatcattccccATGCAGAAACTAAGACATC
				Rv	agaattcggatcccTTAAAGCCGGCTACTGATG
Gray bichir	*aqp10.2*	XM_039751813.1	In-Fusion cloning	Fw	gcagatcattccccATGGAGAAAGTGTTTAAAG
				Rv	agaattcggatcccTTAAAACCTATTGACAATAC
West African lungfish	*aqp10*	XM_044080642.1	In-Fusion cloning	Fw	gcagatcattccccATGCTTTCATACCCACCACA
				Rv	agaattcggatcccCTAAGTACCCATTATTATGT
African clawed frog	*aqp7.L*	XM_018226930.2	RT-PCR	Fw	CTGGATACGCCATCAACCCAG
				Rv	CCACTTTGGTCTCTTCTTCCTCC
African clawed frog	*aqp8.L*	XM_018237062.2	RT-PCR	Fw	AAATCATGCCCCACTGGTTTGAC
				Rv	CAGCAGGATTAAAATGGCCACC
African clawed frog	*aqp9.L*	XM_018253027.2	RT-PCR	Fw	GGGATGTGCAATGAATCCTGC
				Rv	GGGTATCTTCCATGTCATTGCTG
African clawed frog	*actb.L*	NM_001088953.2	RT-PCR	Fw	GACAGTCTGTGTGCGTCCAA
				Rv	TGGGCGACCCACAATAGATG
Spotted gar	*actb*	XM_006637121.2	RT-PCR	Fw	TGCCGCACTGGTTGTTGATA
				Rv	GAAGCTGTAGCCTCTCTCGG

Supplementary Table S2. Amino acid sequences of Aqp10s used for the phylogenetic analysis.

Gene	Species	Accession number
aqp10	Human (*Homo sapiens*)	NP_536354
aqp10	Pig (*Sus scrofa*)	NP_001121926
aqp10	Chicken (*Gallus gallus domesticus*)	XP_015154084
aqp10	Japanese gecko (*Gekko japonicus*)	XP_015274582.1
aqp10	African clawed frog (*Xenopus laevis*)	XP_041429683.1
aqp10	Western clawed frog (*Xenopus tropicalis*)	XP_017945847
aqp10	West African lungfish (*Protopterus annectens*)	XP_043936577.1
aqp10.1	spotted gar (*Lepisosteus oculatus*)	LC767942
aqp10.2	spotted gar (*Lepisosteus oculatus*)	LC767946
aqp10.1a	zebrafish (*Danio rerio*)	NP_001002349
aqp10.2b	zebrafish (*Danio rerio*)	XP_005159449
aqp10.1a	channel catfish (*Ictalurus punctatus*)	ENSIPUT00000006294.1
aqp10.2b	channel catfish (*Ictalurus punctatus*)	ENSIPUT00000011195.1
aqp10.1a	allis shad (*Alosa alosa*)	XM_048261394
aqp10.2a	allis shad (*Alosa alosa*)	XM_048261395
aqp10.2b	allis shad (*Alosa alosa*)	XM_048229129
aqp10.1a	Atlantic herring (*Clupea harengus*)	ENSCHAT00000039518.1
aqp10.2a	Atlantic herring (*Clupea harengus*)	ENSCHAT00000037340.1
aqp10.2b	Atlantic herring (*Clupea harengus*)	ENSCHAT00000034239.1
aqp10.1a	Atlantic cod (*Gadus morhua*)	ENSGMOT00000031448.1
aqp10.1b	Atlantic cod (*Gadus morhua*)	ENSGMOT00000011855.2
aqp10.2b	Atlantic cod (*Gadus morhua*)	ENSGMOT00000045998.1
aqp10.1a	electric eel (*Electrophorus electricus*)	ENSEEET00000015527.1
aqp10.1b	electric eel (*Electrophorus electricus*)	ENSEEET00000013246.1
aqp10.2b	electric eel (*Electrophorus electricus*)	ENSEEET00000013398.1
aqp10.1a	Japanese pufferfish (*Takifugu rubripes*)	LC735291
aqp10.2b	Japanese pufferfish (*Takifugu rubripes*)	LC735292

Supplementary Table S3. Genome databases used for the synteny analysis.

Species	Genome database	Reference
Human (*Homo sapiens*)	GCF_000001405.40	(Lander, et al. 2001)
Mouse (*Mus musculus*)	GCF_000001635.27	(Mouse Genome Sequencing, et al. 2002)
Pig (*Sus scrofa*)	GCF_000003025.6	(Groenen, et al. 2012)
Chicken (*Gallus gallus domesticus*))	GCF_016699485.2	(International Chicken Genome Sequencing 2004)
Japanese gecko (*Gekko japonicus*)	GCF_001447785.1	(Liu, et al. 2015)
African clawed frog (*Xenopus laevis*)	GCF_017654675.1	(Session, et al. 2016)
Coelacanth (*Latimeria chalumnae*)	GCF_000225785.1	(Amemiya, et al. 2013)
West African lungfish (*Protopterus annectens*)	GCF_019279795.1	(Wang, et al. 2021)
Gray bichir (*Polypterus senegalus*)	GCF_016835505.1	(Bi, et al. 2021)
Spotted gar (*Lepisosteus oculatus*)	GCF_000242695.1	(Braasch, et al. 2016)
Atlantic herring (*Clupea harengus*)	GCF_900700415.2	(Martinez Barrio, et al. 2016)
Allis shad (*Alosa alosa*)	GCF_017589495.1	(Sabatino, et al. 2022)
Zebrafish (*Danio rerio*)	GCF_000002035.6	(Howe, et al. 2013)
Channel catfish (*Ictalurus punctatus*)	GCF_001660625.3	(Chen, et al. 2016)
Electric eel (*Electrophorus electricus*)	GCF_013358815.1	(Gallant, et al. 2014)
Atlantic cod (*Gadus morhua*)	GCF_902167405.1	(Star, et al. 2011)
Japanese medaka (*Oryzias latipes*)	GCF_002234675.1	(Kasahara, et al. 2007)
Nile tilapia (*Oreochromis niloticus*)	GCF_001858045.2	(Brawand, et al. 2014)
Japanese pufferfish (*Takifugu rubripes*)	GCA_901000725.3	(Aparicio, et al. 2002)

Amemiya CT, et al. 2013. The African coelacanth genome provides insights into tetrapod evolution. Nature 496: 311-316. doi: 10.1038/nature12027

Aparicio S, et al. 2002. Whole-genome shotgun assembly and analysis of the genome of *Fugu rubripes*. Science 297: 1301-1310.

Bi X, et al. 2021. Tracing the genetic footprints of vertebrate landing in non-teleost ray-finned fishes. Cell 184: 1377-1391 e1314. doi: 10.1016/j.cell.2021.01.046

Braasch I, et al. 2016. The spotted gar genome illuminates vertebrate evolution and facilitates human-teleost comparisons. Nature Genetics 48: 427-437. doi: 10.1038/ng.3526

Brawand D, et al. 2014. The genomic substrate for adaptive radiation in African cichlid fish. Nature 513: 375-381. doi: 10.1038/nature13726

Chen X, et al. 2016. High-quality genome assembly of channel catfish, *Ictalurus punctatus*. Gigascience 5: 39. doi: 10.1186/s13742-016-0142-5

Gallant JR, et al. 2014. Nonhuman genetics. Genomic basis for the convergent evolution of electric organs. Science 344: 1522-1525. doi: 10.1126/science.1254432

Groenen MA, et al. 2012. Analyses of pig genomes provide insight into porcine demography and evolution. Nature 491: 393-398. doi: 10.1038/nature11622

Howe K, et al. 2013. The zebrafish reference genome sequence and its relationship to the human genome. Nature 496: 498-503. doi: 10.1038/nature12111

International Chicken Genome Sequencing C 2004. Sequence and comparative analysis of the chicken genome provide unique perspectives on vertebrate evolution. Nature 432: 695-716. doi: 10.1038/nature03154

Kasahara M, et al. 2007. The medaka draft genome and insights into vertebrate genome evolution. Nature 447: 714-719. doi: 10.1038/nature05846

Lander ES, et al. 2001. Initial sequencing and analysis of the human genome. Nature 409: 860-921. doi: 10.1038/35057062

Liu Y, et al. 2015. *Gekko japonicus* genome reveals evolution of adhesive toe pads and tail regeneration. Nat Commun 6: 10033. doi: 10.1038/ncomms10033

Martinez Barrio A, et al. 2016. The genetic basis for ecological adaptation of the Atlantic herring revealed by genome sequencing. Elife 5. doi: 10.7554/eLife.12081

Mouse Genome Sequencing C, et al. 2002. Initial sequencing and comparative analysis of the mouse genome. Nature 420: 520-562. doi: 10.1038/nature01262

Sabatino SJ, et al. 2022. The genetics of adaptation in freshwater Eurasian shad (Alosa). Ecol Evol 12: e8908. doi: 10.1002/ece3.8908

Session AM, et al. 2016. Genome evolution in the allotetraploid frog *Xenopus laevis*. Nature 538: 336-343. doi: 10.1038/nature19840

Star B, et al. 2011. The genome sequence of Atlantic cod reveals a unique immune system. Nature 477: 207-210. doi: 10.1038/nature10342

Wang K, et al. 2021. African lungfish genome sheds light on the vertebrate water-to-land transition. Cell 184: 1362-1376 e1318. doi: 10.1016/j.cell.2021.01.047

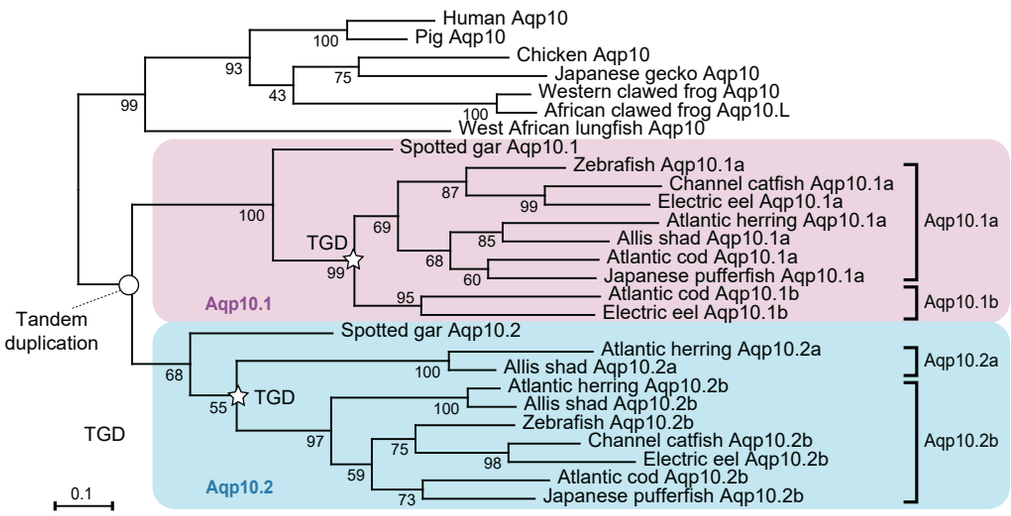

Supplementary Figure S1. Phylogenetic analyses of the amino acid sequences of Aqp10 in bony vertebrates. Vertebrate Aqp amino acid sequences were obtained from the following public databases: Ensembl genome browser (https://www.ensembl.org/) (Martin, et al. 2023), NCBI genome viewer (https://www.ncbi.nlm.nih.gov/genome/gdv/) (Rangwala, et al. 2021) and GenBank/EMBL/DDBJ (Supplementary Table S2). ClustalW (Chenna, et al. 2003) was used to align the amino acid sequences. The alignment composed of 27 sequences and 427 positions was used to construct a maximum-likelihood tree using the MEGA X software (Kumar, et al. 2018) with the JTT model (Jones, et al. 1992). An initial tree for the heuristic search was selected by the NJ/BioNJ method with the JTT model. The tree with the highest log likelihood (-11817.08) is shown. Bootstrap analyses were conducted with 100 bootstrap replicates (Felsenstein 1985).

Chenna R, et al. 2003. Multiple sequence alignment with the Clustal series of programs. Nucleic Acids Res 31: 3497-3500. doi: 10.1093/nar/gkg500

Felsenstein J 1985. Confidence Limits on Phylogenies: An Approach Using the Bootstrap. Evolution 39: 783-791. doi: 10.1111/j.1558-5646.1985.tb00420.x

Jones DT, Taylor WR, Thornton JM 1992. The rapid generation of mutation data matrices from protein sequences. Computer Applications in the Biosciences 8: 275-282. doi: 10.1093/bioinformatics/8.3.275

Kumar S, Stecher G, Li M, Knyaz C, Tamura K 2018. MEGA X: Molecular Evolutionary Genetics Analysis across Computing Platforms. Molecular Biology and Evolution 35: 1547-1549. doi: 10.1093/molbev/msy096

Martin FJ, et al. 2023. Ensembl 2023. Nucleic Acids Res 51: D933-D941. doi: 10.1093/nar/gkac958

Rangwala SH, et al. 2021. Accessing NCBI data using the NCBI Sequence Viewer and Genome Data Viewer (GDV). Genome Research 31: 159-169. doi: 10.1101/gr.266932.120

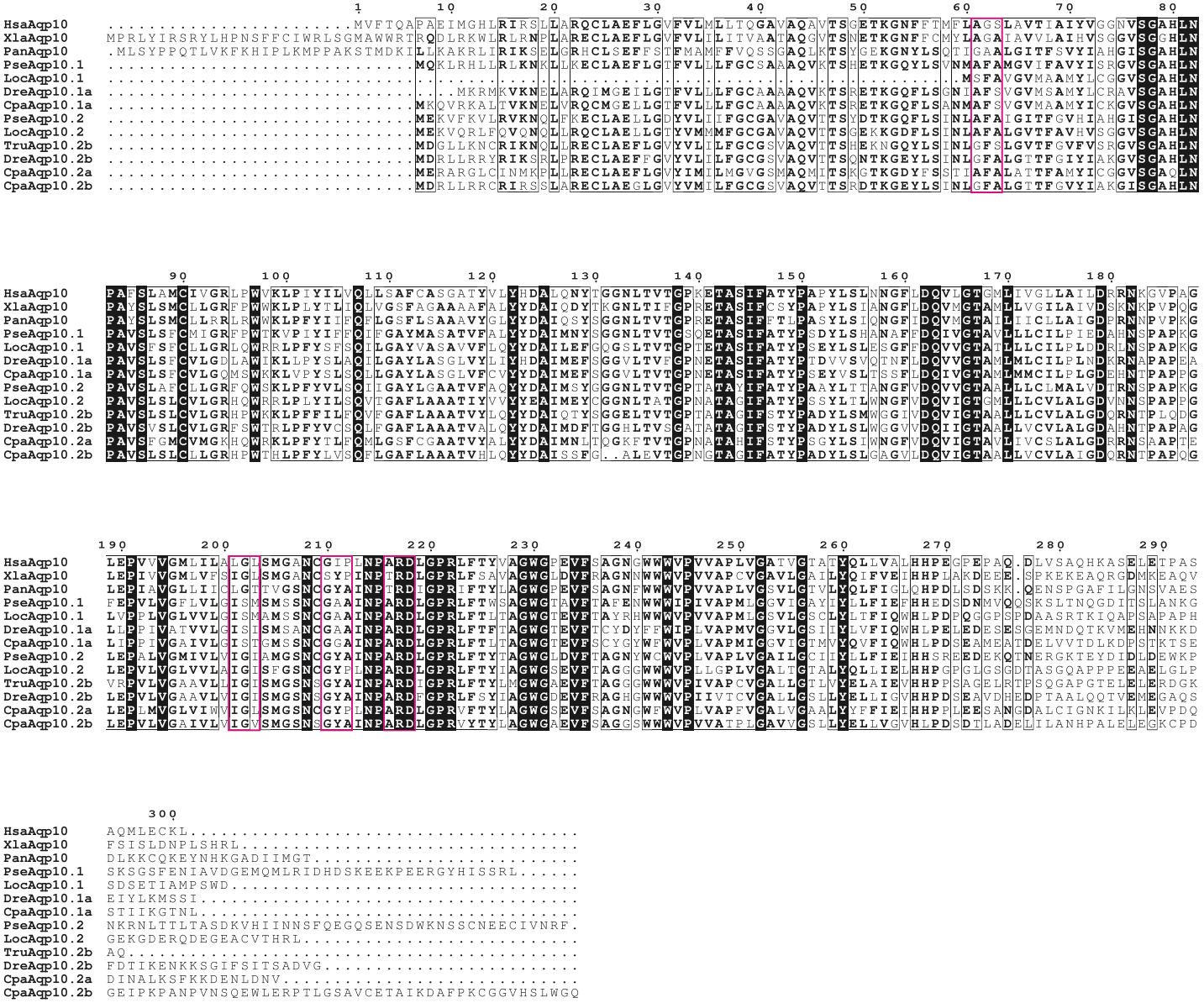

Supplementary Figure S2. Multiple alignment of AQP10 protein sequences. The aromatic/Arg (ar/R) selectivity filters are shown in open magenta boxes. Conserved amino acids are shaded in black. The GenBank accession numbers are described in Supplementary Table S2. Multiple sequence alignment was performed using Clustal W and ESPript (Robert and Gouet 2014) was used to graphically display the results.

Robert X, Gouet P 2014. Deciphering key features in protein structures with the new ENDscript server. Nucleic Acids Res 42: W320-324. doi: 10.1093/nar/gku316